Chemical Kinetics of Radiolabelling Reactions

Holland, Jason P

Abstract: The application of chemical kinetics is one of the most powerful and versatile tools for investigating reaction mechanisms in complex mixtures. Kinetic studies are commonplace in traditional synthetic chemistry but are seldom used in radiopharmaceutical sciences. When deriving standard reaction rate laws, the focus is normally placed on calculating the chemical concentration of different species over time. In radiopharmaceutical synthesis, the desired product is one of the radioactive components of the mixture. Reaction conditions are optimised to obtain the radioactive product in the highest activity yield. When short-lived radionuclides are used, radioactive decay during the reaction window means that the maximum activity yield does not necessarily coincide with the chemical or decay-corrected radiochemical yields. To account for this difference in the kinetic models, it is shown how standard integrated rate laws can be modified to incorporate the contribution from radioactive decay. An example is then presented to show how radiochemical kinetics can be used to model complex systems, like [18F]FDG radiosynthesis, that involve parallel or competing reactions at the different chemical scales of the radionuclide and substrate. Increased knowledge of reaction rates, and a more wide-spread application of radiochemical kinetics, can facilitate the development of new radiolabelling reactions. Accurate identification of maximum activity yields using kinetic models also has the potential to improve the optimisation and radiochemical efficiency of all current and future radiopharmaceutical syntheses.

DOI: https://doi.org/10.1002/chem.201803261

Chemical kinetics of radiolabelling reactions

Jason P. Holland*

University of Zurich, Department of Chemistry, Winterthurerstrasse 190, CH-8057, Zurich, Switzerland

*** Correspondence:**

Prof. Dr Jason P. Holland

Tel: +41.44.63.53.990

E-mail: jason.holland@chem.uzh.ch

Running Title: *Radiochemical kinetics*

One sentence text: *The theory of chemical kinetics is extended to account for radioactive decay during the reaction, and kinetics schemes of clinical-grade radiopharmaceuticals are explored.*

Abstract

The application of chemical kinetics is one of the most powerful and versatile tools for investigating reaction mechanisms in complex mixtures. Kinetic studies are commonplace in traditional synthetic chemistry but are seldom used in radiopharmaceutical sciences. When deriving standard reaction rate laws the focus is normally placed on calculating the chemical concentration of different species over time. In radiopharmaceutical synthesis, the desired product is one of the radioactive components of the mixture. Reaction conditions are optimised to obtain the radioactive product in the highest *activity yield*. When short-lived radionuclides are used, radioactive decay during the reaction window means that the maximum activity yield does not necessarily coincide with the chemical or decay-corrected radiochemical yields. To account for this difference in the kinetic models, it is shown how standard integrated rate laws can be modify to incorporate the contribution from radioactive decay. An example is then presented to show how radiochemical kinetics can be used to model complex systems, like [^{18}F]FDG radiosynthesis, that involve parallel or competing reactions at the different *chemical* scales of the radionuclide and substrate. Increased knowledge of reaction rates, and a more wide-spread application of radiochemical kinetics, can facilitate the development of new radiolabelling reactions. Accurate identification of maximum activity yields using kinetic models also has the potential to improve the optimisation and radiochemical efficiency of all current and future radiopharmaceutical syntheses.

Keywords: Radiochemistry, chemical kinetics, molar activity, pseudo-first-order, second-order, activity yield, fluorine-18, carbon-11, gallium-68, zirconium-89, positron emission tomography (PET).

Introduction

Chemical kinetics is the study of the rate (or velocity) of chemical reactions during which reactants are converted to products along a reaction coordinate.(*1*,*2*) Kinetic experiments usually involve measuring the concentration of a species *versus* time. Other macroscopic or 'classical' variables that influence reaction rates include changes in temperature, pressure, solvent composition, ionic strength, heat and entropy etc. When empirical data on reaction kinetics are combined with thermodynamics, molecular spectroscopy and transition state theory, it allows complex chemical processes to be deconvoluted into the underlying elementary steps that define our concept of reaction mechanisms. Methods derived from statistical thermodynamics can also be used to bridge the gap between the macroscopic and microscopic (or quantum chemical) world. Quantum descriptions allow reaction mechanisms to be explained at the atomic or molecular level. Kinetic investigations that integrate classical and quantum theories are referred to as the study of molecular reaction dynamics.

Kinetic experiments have access to a rich pool of analytical techniques. Traditional methods for monitoring the concentration of a species over time include time-resolved electronic absorption, infrared, NMR or fluorescence-emission spectroscopy, electrochemistry, potentiometry, and radioactive probes coupled with chromatography or chemical separation. The first use of radioactivity to measure kinetics can be traced back to the work of George de Hevesy and the invention of the radiotracer principle in 1923. Later, he received the Nobel Prize in Chemistry in 1943 for using radioactivity to study various chemical processes including transport and metabolism in plants and animals.(*3*–*5*)

Radiotracers are ideally suited for studying kinetics for several reasons.(*6*) First, accurate detection and quantification of radioactivity is possible even when species are present at extremely low concentrations (sub-femtomolar). Second, this high sensitivity means that radiotracers can be used at concentrations that do not perturb the original kinetic (or thermodynamic) process under investigation. Finally, many different radionuclides are available which means that it is possible to select or synthesise radiotracers that are chemically identical to the reacting species. In this respect, organic compounds labelled with ^{3}H($t_{1/2}$ = 12.32 y), ^{14}C($t_{1/2}$ = 5700 y), ^{32}P($t_{1/2}$ = 14.268 d), and ^{35}S($t_{1/2}$ = 87.37 d) are frequently used in drug development to measure target binding properties *in vitro*, as well as absorption, distribution metabolism and excretion *in vivo*. Biological assays that use radiotracers include, for example, the measurement of enzyme-catalysed reactions using ^{32}P- or ^{35}S-labelled adenosine triphosphate.(*7*)

The use of radiopharmaceuticals for diagnostic imaging or molecularly target radionuclide therapy is a core discipline in modern Nuclear Medicine. In contrast to the use of radiotracers in chemical or enzymatic assays, radiopharmaceutical synthesis usually involves working with radionuclides that have comparatively short half-lives.(*8*,*9*) For instance, imaging agents for positron emission tomography (PET) often utilise ^{11}C($t_{1/2}$ = 20.364 min.), ^{13}N($t_{1/2}$ = 9.965 min.), ^{18}F($t_{1/2}$ = 109.7 min.), ^{64}Cu($t_{1/2}$ = 12.701 h), ^{68}Ga($t_{1/2}$ = 67.71 min.), and ^{89}Zr($t_{1/2}$ = 78.41 h). Here, the radioactive product is the desired species. The challenge is that the entire synthetic process must be completed on a time scale that gives sufficient activity for further use in imaging or therapy. Radiopharmaceutical production can be divided into two time-critical steps: *i*) radiochemical synthesis, and *ii*) quality control and release of the isolated product. Optimisation of quality control procedures is beyond the scope of this article. Due to the time constraints, efficient radiopharmaceutical synthesis is strongly dependent on reaction rates. Radiolabelling

reactions are frequently 'optimised' empirically to give the highest decay-corrected radiochemical yield (RCY) in the shortest time, but actual reaction rates (and rate constants) are rarely determined.

The application of advanced chemical kinetics in radiopharmaceutical science has great potential to improve and streamline the process of optimising new (and existing) radiolabelling reactions. The problem is that kinetics models that focus on the *activity* of a radioactive component of the mixture as the primary variable are absent from standard texts.(*1*,*2*,*10–14*) In this perspective, the theory of chemical kinetics is extended to account for radioactive decay during the reaction/process. Analytical solutions and graphical plots are used to illustrate that maximum chemical and radiochemical yields do not coincide with maximum activity yield in first- and second-order radiochemical reactions with short-lived radionuclides. By extension, it is shown that the decay-corrected RCY is not the most appropriate variable to use when optimising these radiolabelling reactions. Finally, examples using data from the clinical production of four PET radiopharmaceuticals: [^{11}C]raclopride,(*15–17*) 2-deoxy-2-[^{18}F]fluoro-D-glucose ([^{18}F]FDG),(*18*) [^{68}Ga]GaPSMA-11,(*19*) and the antibody-based agent [^{89}Zr]Zr-DFO-J591 are presented (Figure 1).(*20–22*) The primary motivation of this work is to show how radiochemistry can be integrated more closely with traditional curricula of the chemical sciences for mutual benefit. Ultimately, a more wide-spread use of chemical kinetics would help radiochemists to identify new reactions that have potential in radiochemistry, and reduce the time spent optimising reactions when new precursors/substrates or reactions become available.

The theory of radiolabelling kinetics

Activity yield as the key variable

Before examining the chemical kinetics of radiolabelling reactions, it is important to define the variables. Current nomenclature rules and parameter definitions given in the consensus report by Coenen *et al.* are used throughout.(*23*) By definition, the RCY is the amount of activity in the product expressed as a percentage (%) of the starting activity used in the considered process (for example, synthesis, separation, etc.), where both quantities refer to the same radionuclide, and are decay corrected to the same point in time before the calculation is performed. The RCY is an important value in radiochemical synthesis, but it is not the most useful variable when studying or optimising radiochemical kinetics where the goal is normally to obtain the maximum *activity* of the desired radioactive product.

Consider a quantitative reaction between a radioactive species (A), and a radiolabelling precursor/substrate (B), that gives a single isolated product (P) with no material losses (Equation 1). The second-order rate constant is given by k_2 (M^{-1} s^{-1}).

$$A + B \overset{k_2}{\rightarrow} P \qquad \text{(Equation 1)}$$

At the end of the reaction, the decay-corrected RCY is equal to the chemical yield (calculated using the radioactive species as the limiting reagent), and both equal 100%. In reactions where no appreciable radioactive decay occurs during the experiment, such as those involving long-lived radionuclides and/or very short reaction times, optimisation based on the chemical yield or decay-corrected RCYs is sufficient. However, in processes where radioactive decay in experimental window in non-negligible (as is the case for the synthesis of many PET radiotracers), decay-

corrected RCYs are insufficient to describe the evolution of the *activity* associated with different radiochemical species over time.

The absolute and relative activity of a radioactive product at any time point is given by the non-decay-corrected activity yield. Activity yield is defined as, '…the overall activity of a radioactive product isolated from the production of a radiolabelled compound or radiopharmaceutical.'(*23*) Activity yields are normally expressed in units of activity (Bq) but values can also be normalised to the initial activity and reported as a percentage (%). This step facilitates comparison with chemical yields (%) and is convenient for kinetic analysis.

It is important to note that the chemical yield and the activity yield differ when radioactive decay is non-negligible during the process. Although high chemical yields are desirable, the maximum activity yield does not necessarily coincide with peak chemical conversion. For instance, once the reaction given by Equation 1 is complete, the chemical yield (and RCY) are 100% at all time points, but the activity yield is time-dependent and decreases by the factor, $A_0 e^{-\lambda t}$. Here, A_0 is the initial activity in Bq, λ / s^{-1} is the decay constant, and t is the time difference between the initial and final activity measurements. A chemically efficient, quantitative reaction is of no use in radiochemical synthesis if it proceeds too slowly and the activity has decayed before the product can be isolated/used. Therefore, optimisation of radiolabelling reactions requires identifying conditions that give the highest activity yield. Methods for calculating activity yields based on standard reaction kinetic schemes are presented in the following sections.

First-order and pseudo-first-order radiochemical reactions

The majority of radiolabelling reactions involve a bimolecular process (Equation 1). Exceptions include Szilard-Chalmers-type processes where a radioactive product is isolated after unimolecular

degradation of an irradiated target material or radioactive parent species. Szilard-Chalmers reactions are not relevant for PET radiochemistry and are not considered further. In addition, the kinetic analysis of first-order reactions follows the same derivation as pseudo-first-order reactions, the latter of which is given below.

Biomolecular reactions can be described by a second-order rate law (Equation 2) where the observed initial rate is dependent on the initial concentrations, $[A]_0$ and $[B]_0$.

$$-\frac{d[A]}{dt} = -\frac{d[B]}{dt} = \frac{d[P]}{dt} = k_2[A][B] \qquad \text{(Equation 2)}$$

In situations where $[B]_0 >> [A]_0$ (normally accepted to be a ~100-fold molar excess of species B in standard kinetic studies), the method of isolation can be used to simplify the analysis *via* the pseudo-first-order approximation (Equation 3; where the observed rate constant, $k_{obs} = k_2[B]_0$).

$$-\frac{d[A]}{dt} = k_{obs}[A] \qquad \text{(Equation 3)}$$

Most radiolabelling reactions can be designed to obey pseudo-first-order kinetics through judicious choice of the starting conditions. However, in later sections it will be shown that data on the clinical production of four different radiopharmaceuticals indicate that caution should be used before making assumptions about the mole ratio of reactants (*vide infra*). Integrated rate laws for a pseudo-first-order reaction that give the *chemical* concentrations [A] and [P] *versus* time are given by Equations 4 and 5, respectively.

$$[A] = [A]_0 e^{-k_{obs}t} \qquad \text{(Equation 4)}$$

$$[P] = [A]_0(1 - e^{-k_{obs}t}) \qquad \text{(Equation 5)}$$

If species A and P are radioactive, the calculation of activity yield requires that concentrations be modified to account for radioactive decay during the reaction. Decay-corrected formulae are given by Equations 6 and 7, where A_X is the activity yield of species X at time t. Values of A_X can be expressed as a percentage by normalising to the initial activity, A_0 at $t = 0$ s.

$$A_{\mathrm{A}} = [\mathrm{A}]e^{-\lambda t} = [\mathrm{A}]_0 e^{-(k_{\mathrm{obs}}+\lambda)t} \qquad \text{(Equation 6)}$$

$$A_{\mathrm{P}} = [\mathrm{P}]e^{-\lambda t} = [\mathrm{A}]_0(1 - e^{-k_{\mathrm{obs}}t}) \cdot e^{-\lambda t} \qquad \text{(Equation 7)}$$

A kinetic plot showing the change in chemical yields of species A, B and P, and the activity yield A_{P} *versus* time is shown in Figure 2A. Starting conditions were defined from the clinical radiosynthesis of [^{18}F]FDG (see Table 1 [*vide infra*], and Supporting Information Table S1). In this example, the theoretical maximum activity yield, A_{P}(max.), is ~82% and occurs at ~24 min., but the maximum chemical conversion (here, where both the chemical yield [P], and RCY, equal 100%) does not occur until ~45 min. Interestingly, when A_{P} reaches a peak, the total activity in the sample is ~86% which means that the radiochemical purity (RCP) is only ~96%. If the reaction is allowed to proceed until complete chemical conversion, the radiochemical purity (RCP) approaches 100% asymptotically, but at the expense of decreasing the theoretical A_{P}(max.) to ~75% at 45 min. These data illustrate the compromise that must be made between activity yields and RCP when optimising radiolabelling reactions.

When new reactions are developed, their potential use in radiochemistry is governed by many factors. These factors include (among others): the chemically efficiency (yield) of the process; accessibility, stability, solubility and reactivity of the radiolabelling precursors; regio- and stereo-selectivity of the products; and functional group tolerance / substrate scope etc. Reaction rates are also crucial in deciding if a new reaction will work in a radiochemical setting. Figure 2B shows the variation in A_{P} *versus* time, as the overall reaction rate changes by variation in k_{obs} from 0.02 s^{-1} to 0.0002 s^{-1}. The rates of inherently slow reactions can be increased by using more precursor, but solubility and competing side reactions often place limits on the maximum value of $[\mathrm{B}]_0$. Clinical syntheses of [^{18}F]FDG use a relatively large amount of precursor (ca. 10 – 30 mg), but such high values are not common in radiochemistry where a secondary goal of optimisation is

to reduce $[B]_0$. Therefore, the data in Figure 2B suggest that for successful application in ^{18}F-radiochemistry, new reactions should aim have observed rate constants for nucleophilic S_N2 substitution by fluoride anions at least ~0.001 M^{-1} s^{-1} (pink line). This lower boundary to the value of k_{obs} ensures that the reaction reaches maximum A_P within a reasonable reaction time of <60 min. To maintain this limit on k_{obs} when using lower amounts of radiolabelling precursor, the inherent reaction rate (given by the value of k_2) in general must be >0.1 M^{-1} s^{-1}.

Similar analyses can be performed for different radionuclides. Pseudo-first-order kinetics calculated using the same starting conditions as employed in Figure 2A, but switching the radionuclide to ^{15}O, ^{13}N, ^{11}C, ^{68}Ga, ^{64}Cu, and ^{89}Zr, are shown in Figures 3A – 3F, respectively. Values of the corresponding A_P(max.) and RCP are given in Supporting Information Table S1. For long-lived radionuclides like ^{89}Zr, and to a lesser extent ^{64}Cu, activity yields mirror closely the chemical yield or RCY in the region before A_P reaches a maximum. For example, when A_P reaches a theoretical peak, corrections for activity yield constitute a difference of <1% for ^{89}Zr, and <4% for ^{64}Cu, *versus* the chemical yield or decay-corrected RCY. Therefore, for most radiolabelling processes that use radionuclides where the physical half-life is >10 times the reaction window, effective reaction optimisation can be accomplished on the basis of standard chemical yields or RCYs, without introducing significant loss of activity in the final product.

For short-lived radionuclides like ^{15}O, ^{13}N, ^{11}C, ^{18}F and ^{68}Ga, a pronounced difference occurs between A_P(max.) and the chemical yield or RCY. Analysis indicates that under otherwise equivalent conditions, for ^{11}C-radiolabelling reaction to achieve a theoretical A_P(max.) of ~90%, the observed reaction rate must increase by a factor of 10 compared with processes that involves ^{18}F. Hence, for applications in radiopharmaceutical synthesis, new ^{11}C-radiolabelling reactions should aim to have higher inherent reactions rates with an approximate value of k_2 >1.0 M^{-1} s^{-1}. A

10-fold increase in rate is readily attainable in ^{11}C- and ^{13}N-radiochemistry, but the situation for ^{15}O is more challenging. The very short half-life of ^{15}O requires that (ideally) the reaction goes to completion in ~10 to ~15 s. This means that only very fast and efficient reactions, with $k_2 > \sim 10^2$ M^{-1} s^{-1} can be considered for radiosynthesis with ^{15}O. To place these rate constants in context, strain-promoted, copper-free 'click' reactions are some of the fastest bioorthogonal reactions known, and are commonly used for imaging applications *in vitro* and *in vivo* using pretargeted strategies.(*24–31*) Reported second-order rate constants between azides or tetrazine derivatives, and various strain-promoted alkene or alkyne reagents range from ca. 0.1 to $>10^3$ M^{-1} s^{-1} (Figure 4).

Second-order radiochemical reactions

It is important to note that for standard biomolecular reactions, the use of a second-order kinetic scheme is almost always correct, even when the reactions are performed under pseudo-first order conditions. Data from the clinical production of [^{68}Ga]GaPSMA-11 and [^{89}Zr]Zr-DFO-J591 indicate that (as performed experimentally) these reactions conform to second-order kinetics (Equation 1 and Table 1 [*vide infra*]). When $[A]_0 \neq [B]_0$, the integrated second-order rate law is given by Equation 8.

$$\ln\left(\frac{[B]}{[A]}\right) = \ln\left(\frac{[B]_0}{[A]_0}\right) - k_2 t \qquad \text{(Equation 8)}$$

Chemical concentrations, [A] and [P], can be derived in the standard fashion,(*1*,*2*) and activity yields of species A and P *versus* time are given by Equations 9, and 10, respectively, (where the constant, $\Delta_0 = [B]_0 - [A]_0$).

$$A_A = [A]e^{-\lambda t} = \frac{\Delta_0 [A]_0}{[B]_0 e^{\Delta_0 k_2 t} - [A]_0} \cdot e^{-\lambda t} \qquad \text{(Equation 9)}$$

$$A_{\mathrm{P}} = [\mathrm{P}]e^{-\lambda t} = \frac{[\mathrm{A}]_0[\mathrm{B}]_0\left(1-e^{\Delta_0 k_2 t}\right)}{[\mathrm{A}]_0-[\mathrm{B}]_0 e^{\Delta_0 k_2 t}} \cdot e^{-\lambda t} \qquad \text{(Equation 10)}$$

From the reaction stoichiometry, and by the law of mass balance, the chemical concentration [B] *versus* time is given by Equation 11.

$$[\mathrm{B}] = \Delta_0 + [\mathrm{A}] \qquad \text{(Equation 11)}$$

Second-order kinetic plots showing the change in the chemical yields of species A, B and P, and the activity yield A_{P} *versus* time are presented in Figures 5A and 5B. Starting conditions were defined from the clinical radiosynthesis of [^{68}Ga]GaPSMA-11 and [^{89}Zr]Zr-DFO-J591 (see Table 1 [*vide infra*] and Supporting Information Table S2).

Most radiolabelling reactions with ^{68}Ga and ^{89}Zr should be modelled as a second-order process. In fact, it is likely that many of optimised radiolabelling reactions that use metal-based radionuclides follow second-order kinetics. The reason for this is simple – radiometal chemists usually perform test reactions to evaluate the molar activity of the radionuclide source, and the final product. On scaling up the reactions for production, starting conditions are usually chosen to ensure that the final RCYs and RCPs are close to 100%. This approach has the potential advantage of eliminating the need to perform lengthy purification steps to increase RCP before the product can be used. Although, even in processes that avoid purification, the presence of other chemical impurities must be tested before a product can be released.

In both preclinical and clinical work, ^{68}Ga-radiolabelling reactions are usually complete within 5 – 10 min, whereas ^{89}Zr-radiolabelling of antibodies requires 45 – 60 min. Kinetic calculations indicate that the radiosynthesis of [^{68}Ga]GaPSMA-11 has a second-order rate constant of approximately $k_2 \sim 10^3$ M^{-1} s^{-1}. Radiolabelling to produce [^{89}Zr]Zr-DFO-J591 occurs at a slightly slower rate with k_2 in the range $\sim 10^2 – 10^3$ M^{-1} s^{-1}. Clinical starting conditions are similar for these two reactions with the total moles of A and B in the range 10 – 30 nmol, and initial activities of

~500 – 1000 MBq. When other factors such as differences in reaction temperature and volume are considered, it appears that radiometallation of the HBED-CC by $^{68}Ga^{3+}$ ions, and desferrioxamine B (DFO) by $^{89}Zr^{4+}$ ions, occur at comparable rates.

The striking feature is that radiometallation with $^{68}Ga^{3+}$ and $^{89}Zr^{4+}$ ions using these acyclic chelates occurs spontaneously at reaction rates that are ~10^2 to ~10^4 times faster than most reactions used in ^{11}C- and ^{18}F-radiochemistry. This is exemplified by the fact that radiometal ion chelation occurs under mild conditions (room temperature) whilst many ^{11}C- and ^{18}F-reactions usually require elevated temperatures to drive product formation. In addition, fewer side-products (both chemical and radiochemical) are observed in metal-based radiochemistry than in normal ^{11}C- and ^{18}F-radiolabelling processes. High reaction rates and efficient chemical conversion mean that for metal-based radiochemistry, initial amounts of precursor B can be reduced to ~10^{-8} mol (where $[B]_0$ ~10^{-5} M; Table 1 [*vide infra*]). These initial starting concentrations are around 10^2 – 10^3 times lower than typical starting concentrations of ^{11}C- and ^{18}F-radiolabelling precursors – consistent with the difference in estimated rate constants.

The reader should note that metal ion complexation reactions are not always rapid. Thermodynamic barriers mean that efficient radiometallation of cyclic chelates like DOTA, and the cross-bridged variant CB-TE2A, with $^{64}Cu^{2+}$ requires heating to around 60 – 95 ^{o}C.(*32*) Nevertheless, the high thermodynamic driving forces for complexation, and the relative kinetic ease of displacing mono- or didentate ligands with multidentate chelates, mean that radiometal ions are often the first choice for accessing radiotracers (like many radiolabelled peptides) that cannot be radiolabelled efficiently with existing ^{11}C- or ^{18}F-chemistry.

Parallel or competing radiochemical reactions

The methods used to derive activity yields in pseudo-first-order and second-order radiolabelling reactions can be readily adapted to any kinetic scheme. As illustrated, some radiolabelling reactions, including ^{68}Ga-radiolabelling of peptides and ^{89}Zr-radiolabelling of antibodies can be considered as 'ideal' in that they go to completion rapidly with essentially no side-product formation. This is not the case for the synthesis of most ^{11}C- and ^{18}F-radiopharmaceuticals where complex mixtures of both radioactive and non-radioactive products are frequently encountered. Modelling the kinetics of complex reactions like the radiosynthesis of [^{18}F]FDG or [^{11}C]raclopride (Figure 1) is non-trivial.

In general, the use of more complex kinetic schemes that involve parallel or competing reactions are required to account for the formation of multiple chemical and radiochemical products. For example, in the clinical radiosynthesis of [^{18}F]FDG, the desired product is the main radioactive component (ca. 50% – 60% RCY in ~50 min.)(*18*) but a number of poorly characterised radiochemical species are also formed. Typical starting conditions in [^{18}F]FDG radiosynthesis obey the pseudo-first-order approximation, where $[B]_0 = \sim 100[A]_0$ (Table 1). At the end of synthesis, the *chemical* component of [^{18}F/^{19}F]FDG in the final reaction mixture constitutes only about ~0.5% to ~1.0%. Stoichiometric studies have also shown that the major chemical species can be assigned to elimination and hydrolysis products, yet a significant fraction (ca. ~25%) of the mass balance is composed of unknown compounds (Figure 6).(*33*)

Under pseudo-first-order conditions where $[B]_0 >> [A]_0$, productive *radiochemical* reactions that give different radioactive species can be decoupled from the main *chemical* degradation pathway of species B. Note: Decoupling is valid as long as the pseudo-first-order approximation holds, but in cases where significant change in [B] occurs, it is safer to treat the radiochemical reaction as a second-order process. A generalised parallel reaction scheme is given

by Equations 12 and 13, where the species P_i are radioactive products formed under pseudo-first-order conditions, and species D_j are non-radioactive 'degradation' products. Equation 13 serves as a simplified example that models the chemical degradation of B as multiple, competing, first-order processes. Degradation pathways such as hydrolysis and elimination usually involve more complex rate laws with pronounced solvent effects and acid/base dependency. With more accurate more experimental data, Equation 13 can be easily modified to account for more complex reactions or an increasing number of competing reactions.

$$A + B \overset{k_i}{\rightarrow} P_i \quad i = 1, 2, \ldots n \qquad \text{(Equation 12)}$$

$$B \overset{k_j}{\rightarrow} D_j \quad j = 1, 2, \ldots n \qquad \text{(Equation 13)}$$

During the time period that pseudo-first-order conditions remain valid, the analytical solution for the activity yield of species A is given by Equation 6 (*vide supra*; note that the second-order integrated law given by Equation 9 can also be used), and that of species P_i is given by Equation 14, where $k' = \sum_{i=1}^{n} k_i$.

$$A_{P_i} = [P_i]e^{-\lambda t} = \frac{k_i[A]_0}{k'}\left(1 - e^{-k'[B]_0 t}\right) \cdot e^{-\lambda t} \qquad \text{(Equation 14)}$$

From stoichiometric studies reported by Brown *et al*., the relative product yields can be used to estimate the ratio of the rate constants between the S_N2 reaction with fluoride and competing reactions of B that lead to elimination, hydrolysis, and other unknown products (Equation 15).

$$\frac{[P_1]}{[P_2]} = \frac{k_1}{k_2} \qquad \text{(Equation 15)}$$

The chemical yields of the main species identified from stoichiometric reactions performed under the same conditions as the radiosynthesis are <5% of [^{19}F]FDG from the desired S_N2 substitution, 29% of α,β-glucose from hydrolysis, and 42% (2*R*,3*R*)-3-hydroxy-2-(hydroxymethyl)-2,3-dihydro-4*H*-pyran-4-one from elimination. The remaining ~24% of the mass balance was

associated with unidentified side-products. From these data, it can be deduced that the S_N2-substitution rate is ~8.4 times slower than the main chemical degradation pathway (elimination) and ~5.8 times slower than hydrolysis pathway that yields glucose. Using these data, combined with the reaction scheme given by Equations 12 and 13, and starting conditions derived from data on the clinical production (Table 1), it is possible to simulate the chemical and radiochemical kinetics of [^{18}F]FDG synthesis. Kinetic plots showing the calculated percentage change in the chemical and activity yields of different species present in the radiopharmaceutical synthesis of [^{18}F]FDG are shown in Figures 7A and 7B, respectively. The model includes four different reaction pathways of species B yielding 'products' $D_1 - D_4$. In Figure 7A, the chemical yield [D_1] is equivalent to the total *chemical* yield of all radioactive products, [P_i], formed from the reaction of A with B. The chemical yields, [D_2] and [D_3] are assigned to the elimination and hydrolysis products, respectively, and [D_4] accounts for the presence of unknown species. From the plot of chemical yields it can be seen that the components of the reaction mixture that are formed by the reaction of A and B constitute only a small fraction of the total chemical content (blue line). The fraction is given by the ratio $[A]_0/[B]_0$, and here is <1%. The time-evolution of the activity yields of radioactive species $P_1 - P_4$ is shown in Figure 7B. Species P_1 is assigned to the desired product [^{18}F]FDG and here is formed in ~67% RCY at completion. Arbitrary species $P_2 - P_4$ are simulated to show how the model can be adapted to incorporate the formation of several unknown radioactive byproducts. Here, clinical production data were used to set the starting conditions, and the maximum activity yield A_{P1} ([^{18}F]FDG) is ~57% at 18 min. This value is consistent with the observed activity yields in [^{18}F]FDG productions.(*18*) Accurate kinetic models depend on the conditions used in an individual radiosynthesis. This example illustrates how a detailed knowledge of chemical kinetics can be used to understand the time evolution of different species in even the

most complex radiolabelling mixtures. Importantly, the methods developed here can be readily adapted to increasingly complex reactions, including those that involve catalysis, phase transfer reagents or generation of reactive species *via* electrochemical or photoactivation processes.

Initial conditions in radiolabelling reactions: defining $[A]_0$

The molar activity problem

Previous sections introduced the theory of radiochemical kinetics but the accuracy of a kinetic model in describing a reacting system relies on knowledge of the starting conditions. In standard, non-radioactive chemical kinetics, the initial concentrations can be controlled easily, but in radiochemistry the situation is more complex. Table 1 contains experimental data on the properties of the radionuclide source (species A), and on the radiochemical syntheses of four prominent PET radiopharmaceuticals: [^{11}C]raclopride,(*15–17*) 2-deoxy-2-[^{18}F]fluoro-D-glucose ([^{18}F]FDG),(*18*) [^{68}Ga]GaPSMA-11,(*19*) and the antibody-based agent [^{89}Zr]Zr-DFO-J591 (Figure 1).(*20–22*) For comparison, preclinical data are also given for [^{89}Zr]Zr-DFO-J591.(*20*)

The starting concentration of precursor $[B]_0$ is usually well-known. The initial activity of species A is also measured routinely. Conversion of the activity of species A into the number of moles (or concentration) requires accurate determination of the molar activity, A_s / MBq nmol^{-1}. For preclinical work with many radioactive metal ions, the *apparent* molar activity can be measured by using isotopic dilution assays.(*34*) In contrast, in most clinical processes that use ^{11}C or ^{18}F, the molar activity of the radionuclide source is not normally measured. Representative molar activities for ^{11}C and ^{18}F (Table 1) were extrapolated from the seminal review by Lapi and Welsh.(*35*) Experimental values for ^{11}C, ^{18}F, ^{68}Ga and ^{89}Zr are between 0.1% to 3.0% of the

theoretical maximum molar activity, A_s(max.) (calculated by Equation 16; where N_A is Avogadro's constant).

$$A_s(\text{max.}) = N_A \cdot \lambda \qquad \text{(Equation 16)}$$

It is important to note that A_s(max.) depends on the half-life. Therefore, care must be taken when comparing the molar activities of different radionuclides. For instance, a molar activity of 43.1 MBq nmol^{-1} of ^{89}Zr is chemically equivalent to the much higher value of 1850 MBq nmol^{-1} of ^{18}F. Isotopic dilution factors (IDFs) account for this difference and allow direct comparisons between different radionuclides (Equation 17).

$$\text{IDF} = \frac{A_s(\text{max.})}{A_s} \qquad \text{(Equation 17)}$$

Except in special stoichiometric circumstances, IDF-values are always ≥1, where higher ratios indicate that the radionuclide sample is diluted with an increasing amount of non-radioactive isotopes. Comparison of the radionuclide IDFs listed in Table 1 indicate that ^{18}F and ^{89}Zr radionuclide sources contain a similar number of non-radioactive isotopes. In the case of ^{89}Zr and other radiometal ions, the apparent (or effective) molar activity measured by chemical methods includes the contribution from other chemically similar metal ions that compete for the chelate. For instance, Fe^{3+} ions successfully compete with ^{89}Zr-radiolabelling reactions for complexation by DFO and other siderophores. As an alternative, induction-coupled plasma mass spectrometry (ICP-MS) can be used to measure the true molar activity for most radiometal ions but this tool is not often available in radiochemical facilities. IDF values for ^{11}C-sources are comparatively high due to the difficulties in removing sources of carbon contaminations from the process.(*35*) IDF values of ^{68}Ga eluted from a standard ^{68}Ge/^{68}Ga generator (Eckert&Ziegler) are estimated be between ca. 500 – 1000, which indicates that there is still considerable scope to improve the molar

activity of most ^{68}Ga-radiotracers. However, the values for ^{68}Ga are comparable to many clinical-grade ^{11}C-radiolabelling reactions.

Reported values of radionuclide molar activity of ^{11}C and ^{18}F show substantial variation for many reasons. For example, the methods and materials used in the cyclotron production are known to have a strong influence on the molar activity.(*35*) Füchtner *et al.*(*36*) demonstrated that systematic cleaning procedures can reduce chemical contaminants in ^{18}F samples.(*36*) However, the other reagents and solvents used in a reaction also introduce contaminants, and additional time constraints make it technically challenging to determine the apparent molar activity at the start of each synthesis. Therefore, the molar activity of a radionuclide source is not a reliable way of defining $[A]_0$ in radiochemical kinetics, and an alternative estimate must be found.

Molar activity of the radiochemical product

In 1:1 stoichiometric reactions (Equation 1), the initial molar activity of the radionuclide gives the theoretical upper limit to the (decay-corrected) molar activity of the final product. However, this upper limit is poorly defined, and the omission of additional contaminants introduced in the reaction mixture mean that this value cannot be used to define $[A]_0$. In contrast, the molar activity of an isolated radiopharmaceutical (P) is measured routinely and includes the contribution from all sources of contaminants present in each individual reaction. Consequently, the product molar activity gives an accurate estimate of the *lower* limit of initial molar activity of species A at $t = 0$ s, and is therefore, a suitable alternative for defining $[A]_0$.

One caveat is that reported molar activities of the product are not always decay-corrected to the start of the experiment. Decay corrections can be performed if the reaction time is documented, but since most PET radiotracer syntheses are completed within one half-life, the use

of non-decay corrected values will only overestimate $[A]_0$ by a factor of ~2. To place this error in context, $[B]_0$ is often systematically varied over ~2 orders of magnitude during radiochemical optimisations. For example, the initial mass of precursor B used in many ^{11}C- and ^{18}F-radiolabelling reactions is in the range 0.1 to 10 mg. Systematic variations and non-reproducible experimental uncertainties in precursor mass are likely to have a larger impact on reaction rates than the aforementioned error that is introduced by estimating $[A]_0$ from molar activity of the isolated products. In the absence of more accurate measurements of molar activities *inside* individual reactions at $t = 0$ s, the use of the product molar activity is recommended for estimating $[A]_0$ in radiochemical kinetics.

Table 1. Representative properties of four clinical-grade PET radiopharmaceuticals radiolabelled with ^{11}C, ^{18}F, ^{68}Ga, or ^{89}Zr.

	Radiopharmaceutical or radiolabelled compound				
Parameter	**[^{11}C]raclopride (clinical)** [a]	**[^{18}F]FDG (clinical)** [b]	**[^{68}Ga]GaPSMA-11 (clinical)** [c]	**[^{89}Zr]Zr-DFO-J591 (clinical)** [d]	**[^{89}Zr]Zr-DFO-J591 (preclinical)** [e]
Properties of the radionuclide source					
Half-life, $t_{1/2}$	20.364 min.	109.7 min.	67.71 min.	78.41 h	78.41 h
Half-life, $t_{1/2}$ (s)	1221.8	6582.0	4062.6	282276.0	282276.0
Decay constant, λ (s^{-1})	5.6730×10^{-4}	1.0531×10^{-4}	1.7062×10^{-4}	2.4556×10^{-6}	2.4556×10^{-6}
Radionuclide reagent	$[^{11}C]CH_3I$ or $[^{11}C]CH_3OTf$	$[^{18}F][K(K_{222})]F$	$[^{68}Ga][Ga(H_2O)_6]Cl_3$	$[^{89}Zr][Zr(C_2O_4)_4]^{4-}$	$[^{89}Zr][Zr(C_2O_4)_4]^{4-}$
Radionuclide molar activity (MBq $nmol^{-1}$)	555 – 1850 [f]	1850 [g]	100 – 200 [h]	17 – 45 [i]	17 – 45 [i]
Theoretical maximum molar activity, A_s (max.) (MBq $nmol^{-1}$)[h]	341626.75	63417.39	102745.34	1478.74	1478.74
Isotopic dilution factor (IDF)	615.5 – 184.7	34.3	1027.5 – 513.7	87.0 – 32.9	87.0 – 32.9
Properties of the radiopharmaceutical synthesis					
Initial activity (MBq)	37000 (1 Ci)	37000 (1 Ci)	1000	555	153.2
Precursor mass (mg)	1.0	10	0.01	3	0.84
Precursor molecular weight (g mol^{-1})	333.21	480.37	947.0	~150,000	~150,000
Nanomoles of precursor B at $t = 0$ s (nmol)	3.00×10^3	2.08×10^4	10.6	20 (antibody)	5.6 (antibody)
No. of chelates per mAb	Not applicable	Not applicable	Not applicable	1.0 – 1.5	3.9

Nanomoles of chemically accessible chelate (nmol)	Not applicable	Not applicable	Not applicable	20.0 – 30.0	21.84
Typical reaction time (min)	0.5 – 5 (HPLC loop) 5 – 20 (vial)	5 – 45	5 – 10	45 – 60	45 – 60
Total production time (min)	30 – 45	30 – 90	30 – 45	60 – 120	60 – 120
Molar activity of the isolated product (MBq $nmol^{-1}$)	770	185	100	23.3	7.01
IDF	443.7	342.8	1027.5	63.5	210.9
Percentage of A_s (max)	0.23%	0.29%	0.10%	1.58%	0.47%
Nanomoles of radioactive species A at t = 0 s (nmol)	48.1	200	10.0	23.8	21.85
Mole ratio (B_0 / A_0) at t = 0 s	62.5	104.1	1.06	0.84 – 1.26 [j]	1.00 [j]
Theoretical maximum RCY (decay corrected)	100%	100%	100%	84% – 100% [j]	100% [j]
Reported isolated RCY (decay corrected)	3.0%	50% – 60%	>98%	70% – 100%	77%

[a] Data on [^{11}C]raclopride were provided by Prof. Neil Vasdev and Dr Armando Garcia, Centre for Addiction and Mental Health, University of Toronto, Canada, and also adapted from the recent work of Shao *et al.*(*15*)

[b] Data on the nucleophilic synthesis of [^{18}F]FDG using the mannose triflate precursor(*18*) were provided Dr Lee Collier, Advion Inc., Ithaca, New York, USA.

[c] Data on the clinical production of [^{68}Ga]Ga-PSMA-11 were provided by Dr Mark Bartholomä, University Hospital Freiburg, Germany, and selected data used from reference (*37*).

[d] Data on the clinical production of [^{89}Zr]Zr-DFO-J519 were provided by Dr Serge Lyashchenko and Prof. Jason S. Lewis, Memorial Sloan-Kettering Cancer Center, New York, USA. Equivalent data were also observed for the clinical production of [^{89}Zr]Zr-DFO-trastuzumab.(*38*)

[e] Data on the preclinical production of [^{89}Zr]Zr-DFO-J519 are from reference (*20*).

[f] The range is based on an assessment of typical molar activities reported by Lapi and Welch(*35*), and in the work of Larsen *et al*.(*39*)

[g] Füchtner *et al.*(*36*) reported a value of 43.0 GBq nmol^{-1} (IDF ~1.5; equivalent to ~68% of the theoretical maximum, A_s) for the molar activity of [^{18}F]fluoride anions produced by the ^{18}O(p,n)^{18}F nuclear transmutation reaction using [^{18}O]H_2O.(*35*,*40*) A more realistic value is 1850 – 3700 MBq nmol^{-1} for the [^{18}F]fluoride anion source (IDF between 34.3 – 17.1; equivalent to between 2.9% and 5.8% of the theoretical maximum molar activity, A_s).

[h] Holland and Bartholomä, unpublished data.

[i] Holland *et al*.(*34*)

[j] Note that the mole ratio and theoretical maximum yields for work with antibodies are calculated based on the number of moles of accessible chelates. This value is equal to the number of moles of antibody, n(mAb), multiplied by the experimentally measured number of accessible chelates per mAb.

Radiolabelling reaction rates

How fast are current radiopharmaceutical reactions? By using radiochemical kinetic models coupled with the starting conditions given in Table 1, it is possible to estimate how fast a reaction must be for it to be potentially useful in radiopharmaceutical synthesis. The estimated ranges of observed second-order rate constants (k_2-values) derived from radiolabelling reactions using ^{11}C, ^{18}F, ^{68}Ga and ^{89}Zr are shown in Figure 8. The estimated k_2-values of ^{18}F-fluorination reactions show a wide range of reaction rates. This is consistent with the diverse chemistry used in typical S_N2-substitution reactions which are strongly dependent on the reaction conditions, the solvent composition, ionic strength, and the chemical nature of the substrate and the leaving group. Furthermore, ^{18}F-fluoriantion reactions are often performed using catalysts or phase transfer reagents that can strongly influence reaction mechanisms and rate constants. For these reasons, modelling the kinetics of a broad range ^{18}F-radiolabelling reactions is likely to present additional challenges beyond those faced in most other areas of radiochemistry. In contrast, that majority of ^{11}C-radiolabelling reactions involve methylation of amines, alcohols and thiols using reagents including [^{11}C]CH_3I and [^{11}C]CH_3OTf. Again, the kinetics depend on the conditions, but in general, the nucleophilic substitution reactions employed in the clinical production of many ^{11}C-radiopharmaceuticals proceed at similar rates. This observation is reflected in the narrower distribution of estimated k_2-values for ^{11}C-reactions compared to ^{18}F-radiochemistry. Radiometallation reactions depend on the nature of the chelate/complex but are usually fast with estimated rate constants that can exceed $k_2 > 10^3$ M^{-1} s^{-1}. These values mean that radiolabelling with metal radionuclides can often be performed in stoichiometric ratios leading to second-order kinetics.

When developing new reactions for potential use in radiochemistry, reaction rate is one of the critical factors that will determine if the process can deliver sufficient activity yield. If measured reaction rates fall within the range of existing radiolabelling technologies, it is likely that the new process can be adapted for use in radiopharmaceutical synthesis. Fast reaction rates are usually desirable because they facilitate higher radiochemical conversion and higher isolated activity yields. However, slower or more complex reactions in which the desired radiochemical species is not the main radioactive component of the mixture can also be used when low activity yields are acceptable. For instance, when a single imaging dose is required (ca. ~185 to ~740 MBq), activity yields of <1% may still provide enough product, so long as the reaction can be scaled for use with high initial activities.

Conclusions

Chemical kinetic theory has been extended to describe reactions in which different reactants and products undergo radioactive decay during the observation window. Corrections for radioactive decay are straight-forward, and the methodology can be applied to kinetic schemes of any order or complexity. Evaluation of clinical data on current radiopharmaceutical products reveals that, contrary to common perceptions, not all radiolabelling reactions obey pseudo-first-order kinetics. Second-order kinetic schemes are appropriate for many radiolabelling reactions that involve complexation of $^{68}Ga^{3+}$, $^{89}Zr^{4+}$ and other radiometal ions. Fluorination reactions using [^{18}F]fluoride, and some ^{11}C-radiolabelling reactions are likely to follow pseudo-first-order kinetics but the variability in the molar activity of the radionuclide source, and potential contaminants introduced in the reaction, may switch the kinetics toward second-order. Radiochemical kinetics can be used to model complex reactions, like [^{18}F]FDG radiosynthesis, that involve parallel or

competing processes at both the chemical scale of the precursor, and the radiochemical scale of the radionuclide. Finally, it is hoped that more students of radiochemistry will find radiochemical kinetics useful when developing new radiolabelling reactions and improving current radiopharmaceutical syntheses.

Acknowledgements

JPH thanks Prof. Roger Alberto, Dr Henrik Braband, and the Radiochemistry and Imaging Science research group at the University of Zurich for helpful discussions. JPH is also grateful to Dr Mark Bartholomä, Dr Lee Collier, Dr Serge Lyashchenko, Prof. Jason S. Lewis, Prof. Neil Vasdev and Armando Garcia for generous provision of clinical data. This work was funded in part by the Swiss National Science Foundation (SNSF Professorship PP00P2_163683), the European Research Council (ERC-StG-2015, NanoSCAN – 676904), the Swiss Cancer League (Krebsliga Schweiz; KLS-4257-08-2017), and the University of Zurich.

References

1. Espenson JH. Chemical Kinetics and Reaction Mechanisms. 2nd ed. McGraw-Hill; 1981.
2. House JE. Principles of Chemical Kinetics. 2nd ed. Elsevier; 2007.
3. Hevesy G. The Absorption and Translocation of Lead by Plants A Contribution to the Application of the Method of Radioactive Indicators in the Investigation of the Change of Substance in Plants. *Biochem J*. 1923;17:439–445.
4. Chiewitz O, Hevesy G. Radioactive indicators in the study of phosphorus metabolism in rats. *Nature*. 1935;136:754-755.
5. Cockcroft JD. George De Hevesy. *Biogr Mem Fell R Soc*. 1967;13:125-166.
6. Brown GR, Winkler CA. The Kinetics of an Exchange Reaction Using a Radiochemical Tracer. *J Chem Educ*. 1976;53:461-462.
7. Hastie CJ, McLauchlan HJ, Cohen P. Assay of protein kinases using radiolabeled ATP: A protocol. *Nat Protoc*. 2006;1:968-971.
8. Miller PW, Long NJ, Vilar R, Gee AD. Synthesis of 11C, 18F, 15O, and 13N radiolabels for positron emission tomography. *Angew Chemie - Int Ed*. 2008;47:8998-9033.
9. Holland JP, Williamson MJ, Lewis JS. Unconventional Nuclides for Radiopharmaceuticals. *Mol Imaging*. 2010;9:1-20.
10. Logan SR. Fundamentals of Chemical Kinetics. Longman; 1996.
11. Pilling MJ, Seakins PW. Reaction kinetics. Oxford University Press; 1997.
12. Laidler KJ. Chemical kinetics. In: 3rd ed. New York: Harper Collins; 1987:1-531.
13. Atkins P, Paula J De. Atkins' physical chemistry. 11th ed. Oxford University Press; 2009.
14. Cox BG. Modern Liquid Phase Kinetics. In: Oxford University Press; 1994:1-92.
15. Shao X, Schnau PL, Fawaz M V, Scott PJH. Enhanced radiosyntheses of [11C]raclopride

and [11C] DASB using ethanolic loop chemistry. *Nucl Med Biol*. 2013;40:109-116.

16. Iwata R, Pascali C, Bogni A, Miyake Y, Yanai K, Ido T. A simple loop method for the automated preparation of [11C]raclopride from [11C]methyl triflate. *Appl Radiat Isot*. 2001;55:17-22.

17. Fei X, Mock BH, DeGrado TR, et al. An improved synthesis of PET dopamine D2 receptors radioligand [11c]raclopride. *Synth Commun*. 2004;34:1897-1907.

18. Hamacher K, Coenen HH, Stocklin G. Synthesis D-Glucose Using Aminopolyether Supported Nucleophilic Substitution. 1986;27:235-239.

19. Eder M, Schäfer M, Bauder-Wüst U, et al. 68Ga-complex lipophilicity and the targeting property of a urea-based PSMA inhibitor for PET imaging. *Bioconjug Chem*. 2012;23:688-697.

20. Holland JP, Divilov V, Bander NH, Smith-Jones PM, Larson SM, Lewis JS. 89Zr-DFO-J591 for ImmunoPET of Prostate-Specific Membrane Antigen Expression In Vivo. *J Nucl Med*. 2010;51:1293-1300.

21. Morris MJ, Pandit-Taskar N, Carrasquillo JA, et al. Phase I trial of zirconium 89 (Zr89) radiolabeled J591 in metastatic castration-resistant prostate cancer (mCRPC). *J Clin Oncol*. 2013;31.

22. Pandit-Taskar N, O'Donoghue JA, Beylergil V, et al. 89Zr-huJ591 immuno-PET imaging in patients with advanced metastatic prostate cancer. *Eur J Nucl Med Mol Imaging*. 2014;41:2093-2105.

23. Coenen HH, Gee AD, Adam M, et al. Consensus nomenclature rules for radiopharmaceutical chemistry — Setting the record straight. *Nucl Med Biol*. 2017;55:v-xi.

24. De Almeida G, Sletten EM, Nakamura H, Palaniappan KK, Bertozzi CR. Thiacycloalkynes for copper-free click chemistry. *Angew Chemie - Int Ed*. 2012;51:2443-2447.

25. Devaraj NK, Weissleder R. Biomedical applications of tetrazine cycloadditions. *Acc Chem Res*. 2011;44:816-827.

26. Devaraj NK, Weissleder R, Hilderbrand S a. Tetrazine-Based Cycloadditions : Application to Pretargeted Live Cell Imaging. *Communications*. 2008;19:2297-2299.

27. Yang J, Šečkute J, Cole CM, Devaraj NK. Live-cell imaging of cyclopropene tags with fluorogenic tetrazine cycloadditions. *Angew Chemie - Int Ed*. 2012;51:7476-7479.

28. Darko A, Wallace S, Dmitrenko O, et al. Conformationally strained trans-cyclooctene with improved stability and excellent reactivity in tetrazine ligation. *Chem Sci*. 2014;5:3770-3776.

29. Karver MR, Weissleder R, Hilderbrand SA. Bioorthogonal reaction pairs enable simultaneous, selective, multi-target imaging. *Angew Chemie - Int Ed*. 2012;51:920-922.

30. Zeglis BM, Davis CB, Aggeler R, et al. Enzyme-mediated methodology for the site-specific radiolabeling of antibodies based on catalyst-free click chemistry. *Bioconjug Chem*. 2013;24:1057-1067.

31. Zeglis BM, Sevak KK, Reiner T, et al. A Pretargeted PET Imaging Strategy Based on Bioorthogonal Diels–Alder Click Chemistry. *J Nucl Med*. 2013;54:1389-1396.

32. Lebedev AY, Holland JP, Lewis JS. Clickable bifunctional radiometal chelates for peptide labeling. *Chem Commun*. 2010;46:1706.

33. Brown LJ, Ma N, Bouvet DR, et al. Synthesis of the positron-emitting radiotracer [18F]-2-fluoro-2-deoxy-d-glucose from resin-bound perfluoroalkylsulfonates. *Org Biomol Chem*.

2009;7:564-575.

34. Holland JP, Sheh Y, Lewis JS. Standardized methods for the production of high specific-activity zirconium-89. *Nucl Med Biol*. 2009;36:729-739.

35. Lapi SE, Welch MJ. A historical perspective on the specific activity of radiopharmaceuticals: What have we learned in the 35 years of the ISRC? *Nucl Med Biol*. 2012;39:601-608.

36. Füchtner F, Preusche S, Mäding P, Zessin J, Steinbach J. Factors affecting the specific activity of [18F]fluoride from a [18O]water target. *Nuklearmedizin*. 2008;47:116-119.

37. Gourni E, Pozzo L Del, Bartholoma M, et al. Radiochemistry and Preclinical PET Imaging of 68Ga-Desferrioxamine Radiotracers Targeting Prostate-Specific Membrane Antigen. 2017;16:1-11.

38. Holland JP, Caldas-Lopes E, Divilov V, et al. Measuring the pharmacodynamic effects of a novel Hsp90 inhibitor on HER2/neu expression in mice using 89Zr-DFO-trastuzumab. *PLoS One*. 2010;5:e8859.

39. Larsen P, Ulin J, Dahlstrom K, Jensen M. Synthesis of [11C]Iodomethane by Iodination of [11C]Methane. *Appl Radiat Isot*. 1997;48:153-157.

40. Schlyer DJ, Firouzbakht ML, Wolf AP. Impurities in the [18O]water target and their effect on the yield of an aromatic displacement reaction with [18F]fluoride. *Appl Radiat Isot*. 1993;44:1459-1465.

Figure legends

Figure 1. Chemical structures of the radiopharmaceuticals [^{11}C]raclopride, [^{18}F]FDG, [^{68}Ga]GaPSMA-11, and the antibody-based agent [^{89}Zr]Zr-DFO-J591.

Figure 2. (A) Plot showing the change in chemical yields of species A, B and P, and the activity yield of P *versus* time under pseudo-first-order kinetics. Starting conditions were defined by data on the clinical production of [^{18}F]FDG. Note the difference between radioactive decay at time t (black line) and the activity yield $A_P(t)$ is a measure of the radiochemical purity of species P. (B) Plot showing the change in activity yield, A_P, as the reaction rate decreases from k_{obs} = 0.02 to 0.0002 s^{-1} (where $[B]_0$ = 20.8 mM).

Figure 3. Pseudo-first-order kinetic plots illustrating the effect of using radionuclides with different half-lives on the chemical and activity yields of species A, B and P *versus* time. Starting conditions are identical to those used in Figure 2A. (A) ^{15}O ($t_{1/2}$ = 122.24 s). (B) ^{13}N ($t_{1/2}$ = 9.965 min.). (C) ^{11}C ($t_{1/2}$ = 20.364 min.). (D) ^{68}Ga ($t_{1/2}$ = 67.71 min.). (E) ^{89}Zr ($t_{1/2}$ = 78.41 d). NB: for the ^{89}Zr plot, the curves for [P] (blue) and A_P (pink), as well as the curves for radioactive decay (black) and $[B]_0$ (green) overlap in this experimental window.

Figure 4. Structures of several prominent bioorthogonal reagents used in fast, strain-promoted copper-free 'click' conjugation reactions *in vitro* and *in vivo*.(*25*,*31*) Reactions between azides and strained cyclooctynes have rate constants (k_2) between 0.1 – 1.0 M^{-1} s^{-1}, whereas *trans*-cyclooctenes react with tetrazine derivatives under aqueous condition with rate constants >10^3 M^{-1} s^{-1}.(*24*,*28*)

Figure 5. Second-order kinetic plots showing the change in chemical yields of species A, B and P, and activity yield A_P *versus* time. Plots were calculated using data derived from the clinical production of: (A) [^{68}Ga]GaPSMA-11, and (B) [^{89}Zr]Zr-DFO-J591. Second-order rate constants are shown inset (Table S2).

Figure 6. Reaction scheme showing some of the products formed in the synthesis of [$^{18/19}$F]FDG. Chemical yields are adapted from the work of Brown *et al*.(*33*)

Figure 7. Kinetic plots calculated using preclinical and clinical data on the radiochemical synthesis of [^{18}F]FDG. (A) Percentage change in the chemical yield of species A, B and D_j *versus* time. Note that [D_1] is equivalent to the total *chemical* concentration, [P](total), of all species formed by the reaction of A with B, the main component of which is assigned to S_N2 substitution leading to [^{18}F]FDG. Species D_2, D_3 and D_4 are assigned to reactions that yield the elimination, hydrolysis and unidentified products, respectively, from the chemical degradation of precursor B. (B) Percentage change in the activity yields of species A and P_i *versus* time. Species P_1 is equivalent to the desired [^{18}F]FDG product which in this simulation is obtained in ~67% *chemical* yield. Species P_2, P_3 and P_4 are assigned to unidentified radioactive byproducts, and are shown to illustrate how the kinetic scheme can be adjusted to account for parallel/competing radioactive side-reactions.

Figure 8. Chart showing the estimated range of second-order rate constants, k_2 / M^{-1} s^{-1} in successful clinical radiopharmaceutical syntheses using ^{11}C, ^{18}F, ^{68}Ga or ^{89}Zr.

Figure 1.

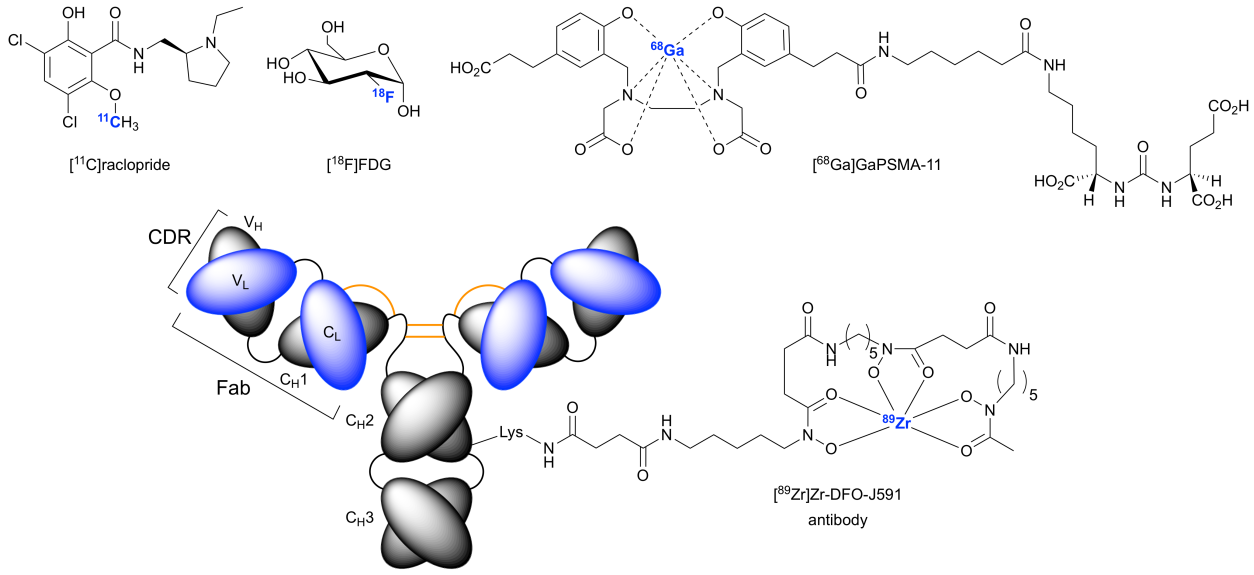
[11C]raclopride
[18F]FDG
[68Ga]GaPSMA-11
CDR
VH
VL
CL
CH1
Fab
CH2
CH3
Lys
89Zr
[89Zr]Zr-DFO-J591
antibody

Figure 2.

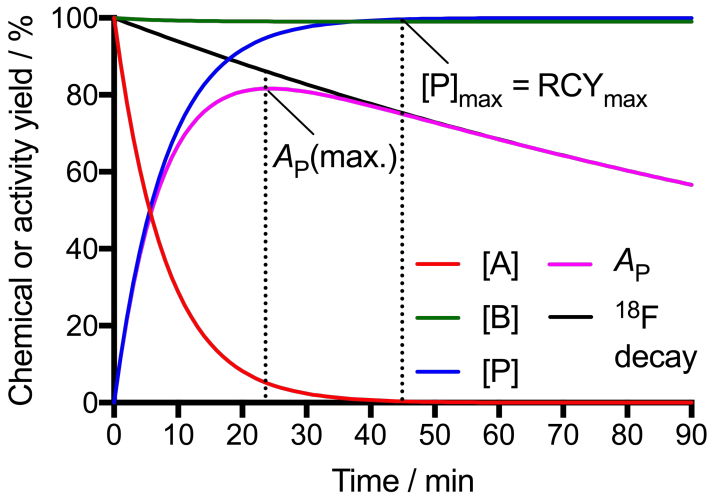
Chemical or activity yield / %
100
80
60
40
20
0
0 10 20 30 40 50 60 70 80 90
Time / min
[P]max = RCYmax
AP(max.)
[A]
[B]
[P]
AP
18F decay

A

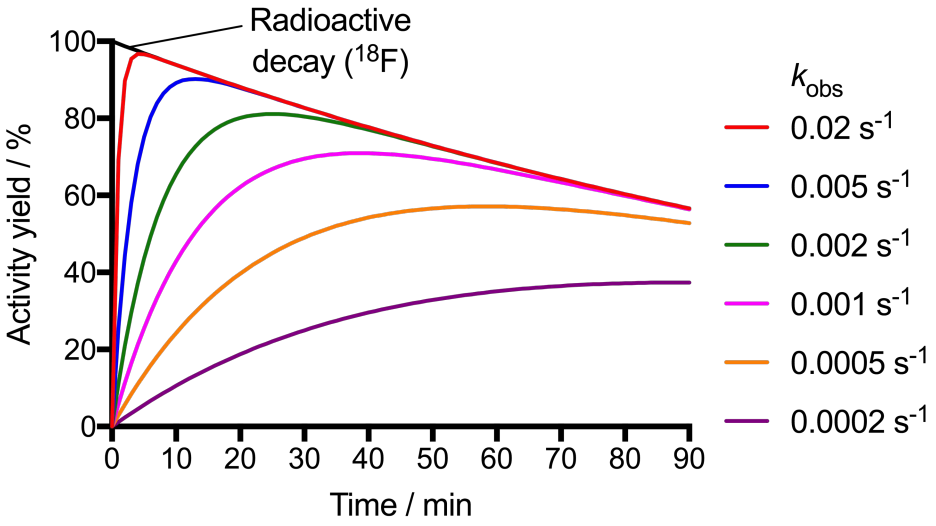
Activity yield / %
100
80
60
40
20
0
0 10 20 30 40 50 60 70 80 90
Time / min
Radioactive decay (18F)
kobs
0.02 s-1
0.005 s-1
0.002 s-1
0.001 s-1
0.0005 s-1
0.0002 s-1

B

Figure 3.

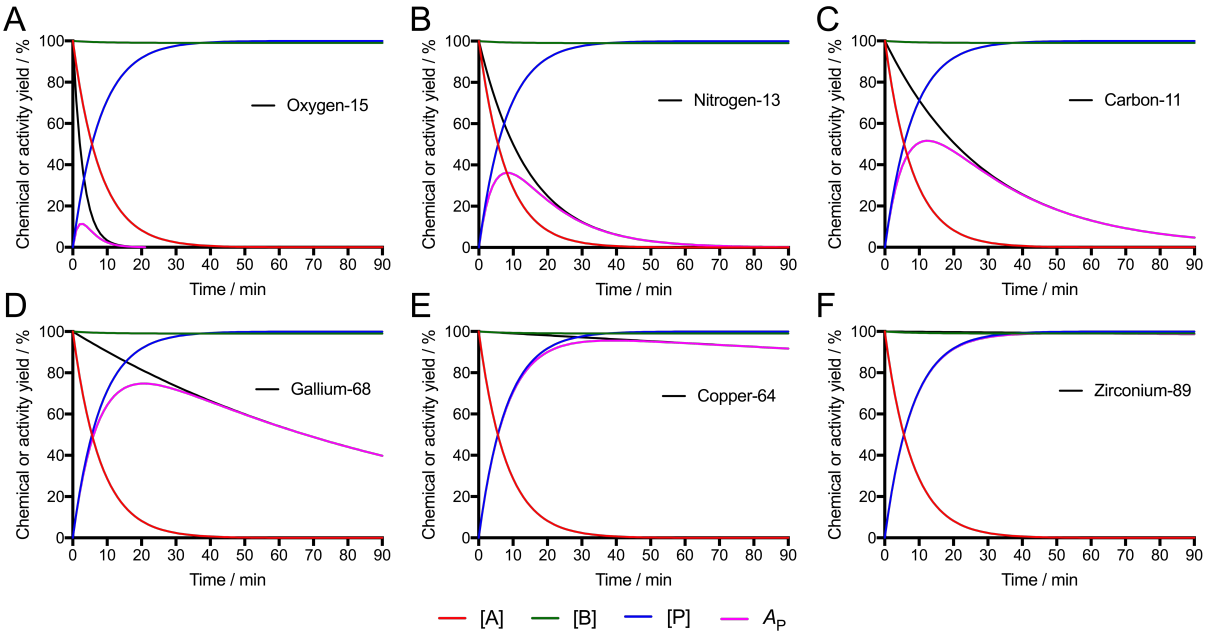
A
B
C
D
E
F
Chemical or activity yield / %
Time / min
Oxygen-15
Nitrogen-13
Carbon-11
Gallium-68
Copper-64
Zirconium-89
[A]
[B]
[P]
A_P

Figure 4.

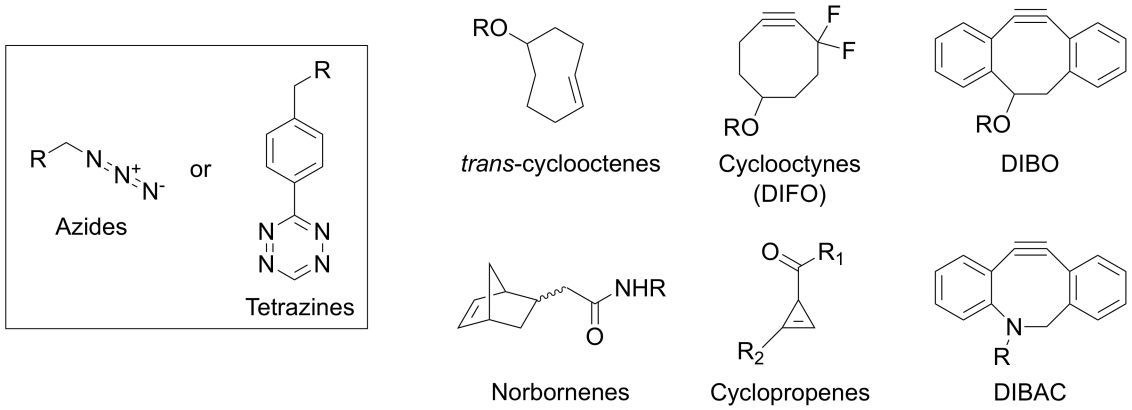
R
N
N+
N-
or
R
N
N
N
N
Azides
Tetrazines
RO
trans-cyclooctenes
F
F
RO
Cyclooctynes
(DIFO)
RO
DIBO
NHR
O
Norbornenes
O
R1
R2
Cyclopropenes
N
R
DIBAC

Figure 5.

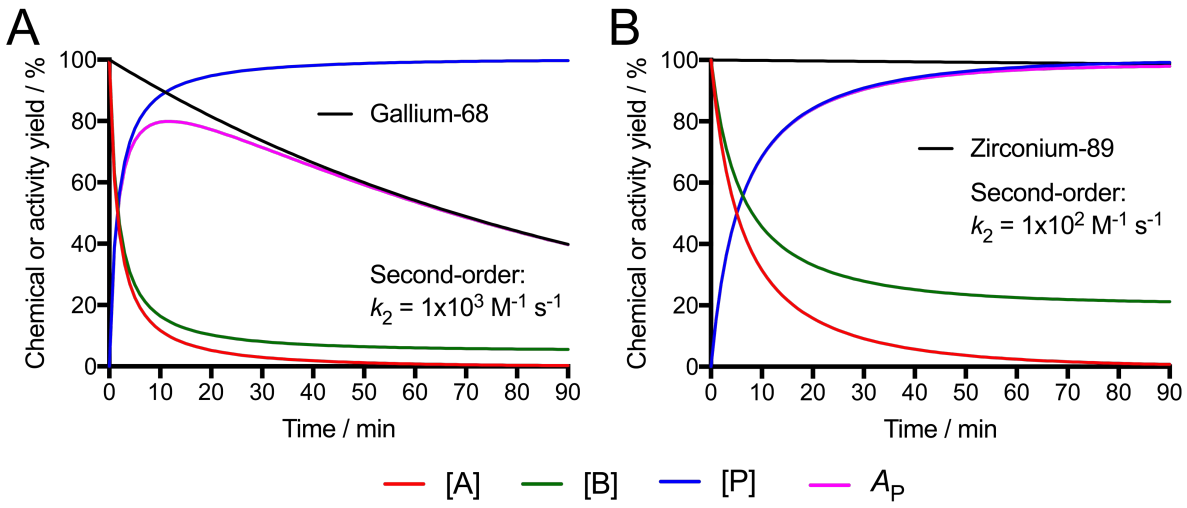
A
B
Chemical or activity yield / %
Time / min
Gallium-68
Second-order:
k_2 = 1x10^3 M^{-1} s^{-1}
Zirconium-89
Second-order:
k_2 = 1x10^2 M^{-1} s^{-1}
[A]
[B]
[P]
A_P

Figure 6.

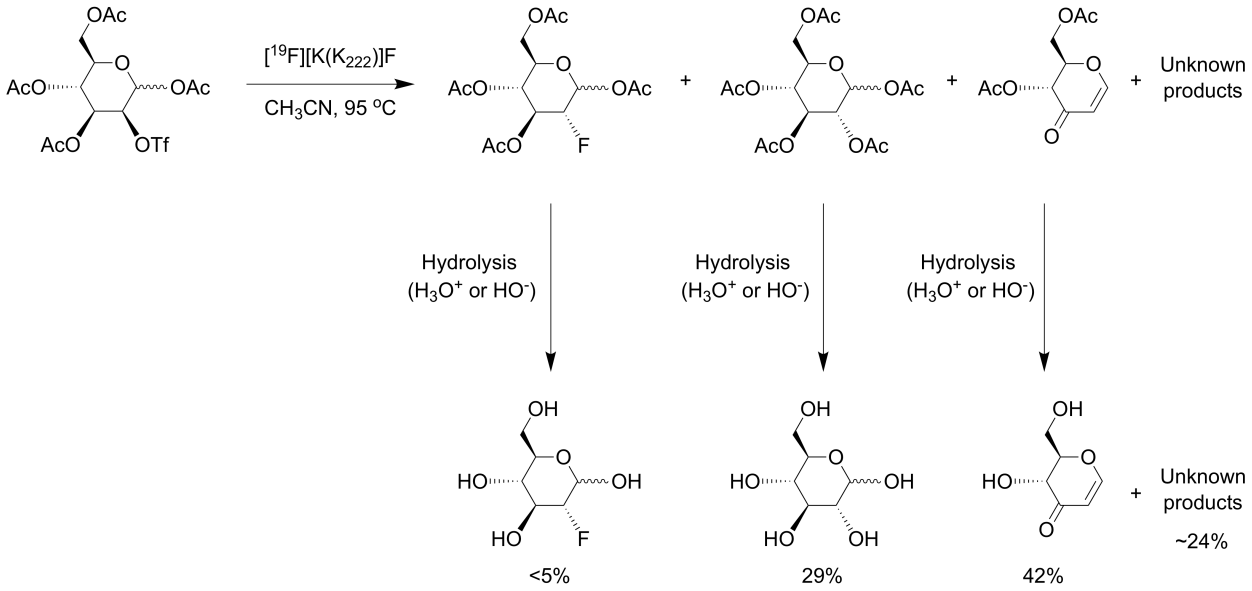
OAc
AcO
OAc
AcO
OTf
[19F][K(K222)]F
CH3CN, 95 °C
F
+
+
+
Unknown products
Hydrolysis (H3O+ or HO-)
Hydrolysis (H3O+ or HO-)
Hydrolysis (H3O+ or HO-)
OH
HO
OH
HO
F
<5%
29%
42%
Unknown products
~24%

Figure 7.

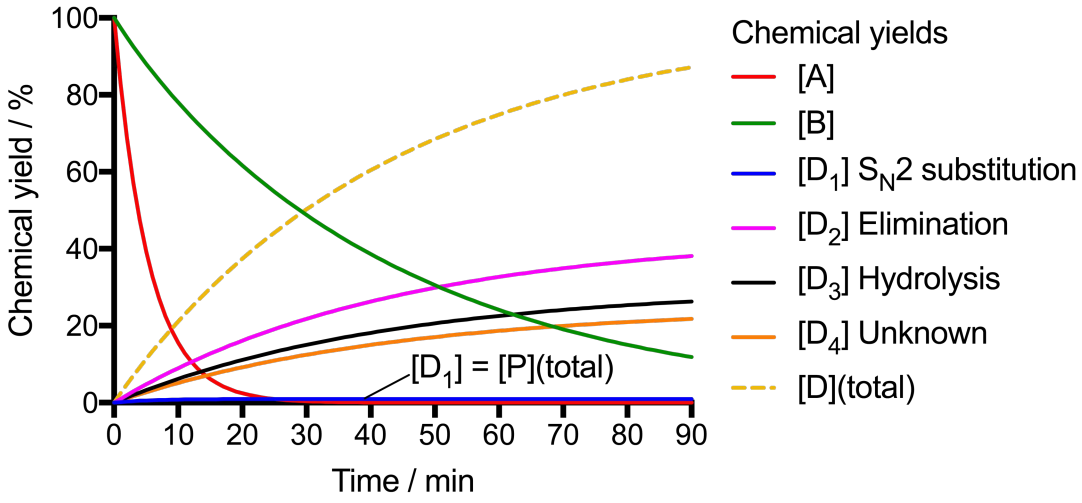
Chemical yield / %
100
80
60
40
20
0
0 10 20 30 40 50 60 70 80 90
Time / min
[D1] = [P](total)
Chemical yields
[A]
[B]
[D1] SN2 substitution
[D2] Elimination
[D3] Hydrolysis
[D4] Unknown
[D](total)

A

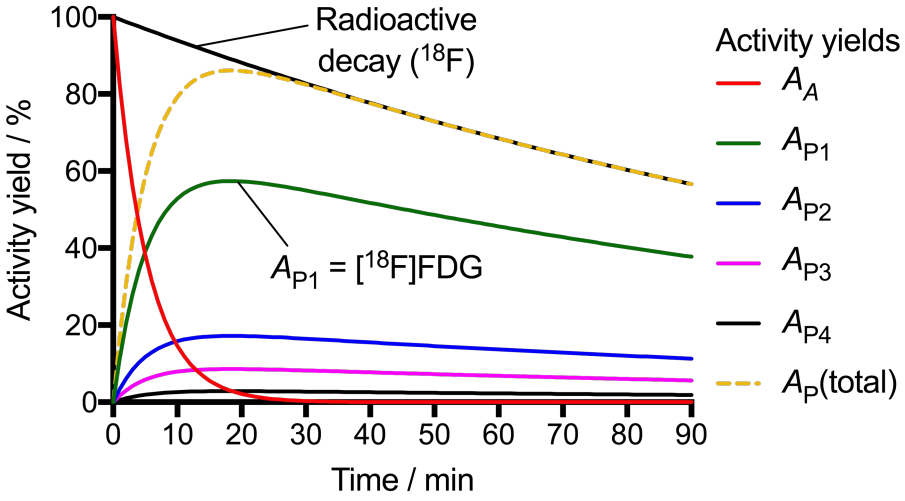
Activity yield / %
100
80
60
40
20
0
0 10 20 30 40 50 60 70 80 90
Time / min
Radioactive decay (18F)
AP1 = [18F]FDG
Activity yields
AA
AP1
AP2
AP3
AP4
AP(total)

B

Figure 8.

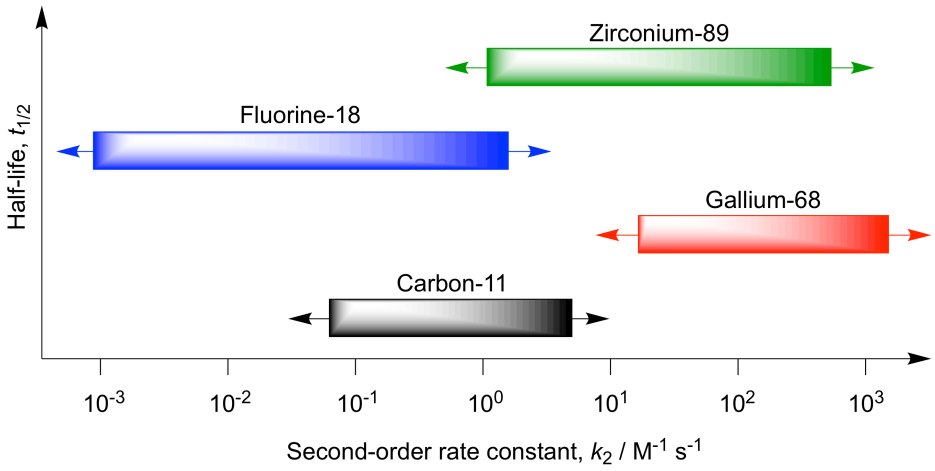
Zirconium-89
Fluorine-18
Gallium-68
Carbon-11
Half-life, $t_{1/2}$
10^{-3}
10^{-2}
10^{-1}
10^{0}
10^{1}
10^{2}
10^{3}
Second-order rate constant, k_2 / M^{-1} s^{-1}